Singlet Fission and Electron Injection from the Triplet Excited State in Diphenylisobenzofuran-Semiconductor Assemblies: Effects of Solvent

Citation for the original published paper (version of record):
Sundin, E., Ringström, R., Johansson, F. et al (2020). Singlet Fission and Electron Injection from the Triplet Excited State in
Diphenylisobenzofuran-Semiconductor Assemblies: Effects of Solvent Polarity and Driving Force.
Journal of Physical Chemistry C, 124(38 Josef Michl Festschrift): 20794-20805.
http://dx.doi.org/10.1021/acs.jpcc.0c06626

THE JOURNAL OF PHYSICAL CHEMISTRY C

pubs.acs.org/JPCC

Article

Singlet Fission and Electron Injection from the Triplet Excited State in Diphenylisobenzofuran–Semiconductor Assemblies: Effects of Solvent Polarity and Driving Force

Published as part of The Journal of Physical Chemistry virtual special issue "Josef Michl Festschrift".

Elin Sundin, Rasmus Ringström, Fredrik Johansson, Betül Küçüköz, Andreas Ekebergh, Victor Gray, Bo Albinsson, Jerker Mårtensson, and Maria Abrahamsson*

Cite This: *J. Phys. Chem. C* 2020, 124, 20794–20805

Read Online

ACCESS | Metrics & More | Article Recommendations | Supporting Information

ABSTRACT: Singlet fission has emerged as a promising way to overcome the Shockley–Queisser limit in solar energy conversion devices, and a few studies have claimed proof-of-principle results using dye-sensitized photoelectrodes. However, a detailed understanding of what factors govern the fate of the excited state on mesoporous surfaces is still lacking. Here, we have studied how the excitation progresses into singlet fission, electron injection, or formation of molecular charge separated states in diphenylisobenzofuran derivatives with flexible carbon linkers attached to nanocrystalline mesoporous ZrO_2, TiO_2, and SnO_2 thin films. We show that singlet fission occurs for the molecule attached to ZrO_2 films when the assembly is immersed in nonpolar solvents, and that singlet fission is hampered by the formation of a molecular charge separated state in more polar solvents. On TiO_2 surfaces, direct electron injection from the singlet excited state outcompetes the singlet fission. Instead, triplet formation occurs via charge recombination from the conduction band of TiO_2 in nonpolar solvents. When the molecule is attached to SnO_2 films, singlet fission partly outcompetes electron injection from the singlet excited state and the two processes occur in parallel. Subsequent to singlet fission on SnO_2, triplet injection into the conduction band of SnO_2 is observed. The results presented here provide a detailed picture of the singlet fission dynamics in molecules attached to mesoporous semiconductor surfaces, demonstrating that both the semiconductor substrate as well as the environment around the molecules have a large impact, which can be useful in the design of future devices.

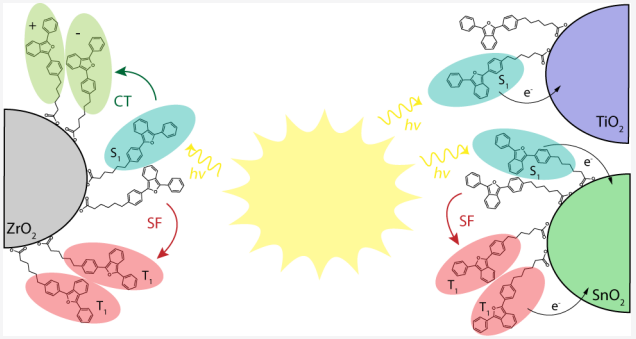

INTRODUCTION

Singlet fission (SF), the spin-allowed process where a molecule in its singlet excited state (S_1) interacts with a neighboring molecule in the ground state to produce two triplet excited states (T_1),[1] was first discovered in the 1960s[2−5] and has attracted a lot of attention over the past 15 years due to the potential for it to increase the efficiency of solar cells.[6,7] If an SF material could be properly integrated into a solar cell, one incident high-energy photon could result in two charge carriers if both created triplets are utilized. This would decrease thermalization losses and lead to an increase compared to the theoretical Shockley–Queisser limit of a single junction solar cell of ∼30%[8] to a new theoretical limit of above 40%.[1,7,9]

Several requirements apply for SF to occur. For example, the energy of the S_1 state needs to be at least twice that of the T_1 state, and proximity between the molecules, as well as a favorable coupling between them, is necessary.[1] The studies over the years have resulted in increased knowledge about design criteria for SF molecules and insights into the mechanism and kinetics of the SF process.[1,6,10−16] SF has traditionally been described to occur through one of two main mechanisms, either involving an observable intermediate charge transfer state or by more direct coupling from the initial singlet excited state into the triplet excited states.[1] In some molecules, an intermediate charge transfer state can facilitate SF,[17,18] whereas in others it appears to inhibit the SF process.[19] The same appears to be true for excimer states: They can either be detrimental to[20,21] or enable SF.[22−25] The exact mechanisms of SF have been thoroughly studied but are not yet fully understood.[16,19,22,26−29] Despite the lack of a

Received: July 20, 2020
Revised: August 23, 2020
Published: August 25, 2020

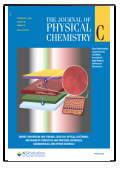

complete mechanistic picture, several examples of efficient SF have been reported in crystalline materials, in thin films, in highly concentrated solutions, and in molecular dimers, displaying quantum yields of triplet formation as high as 150−200%.[18,24,30−33]

Despite the high triplet yields obtained in many SF materials, harvesting the obtained triplets into devices with maintained high yields has proven difficult.[34−36] A few examples of photovoltaic devices with SF material that reaches external quantum efficiencies over 100% exist,[37−39] but the overall efficiency is still far from the desired 200%.

One way to harvest triplets from SF into a device is by attaching the SF molecules to nanocrystalline mesoporous metal oxide surfaces as in dye-sensitized solar cells.[1,35,40] This approach provides the possibility of circumventing the need for long-range triplet diffusion, by injection of electrons from the formed triplet states.[41,42] Another benefit of this approach is the high surface area of the mesoporous surface, providing the ability to attach several molecules in close proximity that could enhance the intermolecular interactions while also allowing for significantly higher light absorption compared to thin films.[43] There are however risks associated with this strategy, including competing singlet electron injection and triplet-charge recombination by neighboring triplets on the surface subsequent to one triplet being injected.[35] The relatively few studies of SF molecules attached to metal oxide surfaces to date have demonstrated that SF can occur on the mesoporous surfaces[41,44−46] as manifested by injection yields over 100%[44] and increased photocurrents.[41,46] This however provides little insight into the mechanism of SF and the complex interplay with fast electron injection from the molecules attached to the mesoporous surfaces.

Derivatives of 1,3-diphenylisobenzofuran (DPIBF), a molecule which displays a triplet yield of 200% in the crystalline phase,[32] have been studied extensively,[17,32,47−51] also attached to nanocrystalline mesoporous metal oxide surfaces.[41,46] Attaching derivatives of DPIBF with carboxylic acid anchoring groups onto core−shell mesoporous electrodes that consist of a TiO_2 core and a ZrO_2[46] or Al_2O_3[41] shell have resulted in enhanced photocurrents with an increasing thickness of the shell. The increase in photocurrent has been attributed to SF and agrees with what would be expected if SF and subsequent electron injection from the triplet state occur. Nevertheless, the overall efficiencies are much lower than what would be expected for an efficient SF system combined with unity electron injection yields. This highlights the need for mechanistic understanding to achieve optimized devices. Hanson and co-workers have studied the photophysical properties of a dicarboxylated DPIBF derivative attached to ZrO_2 thin films and suggested that excimer states and possibly charge separated states between the molecules are populated upon photoexcitation of the DPIBF derivative,[41] which could both compete with and serve as an intermediate step in the SF process. For example, in strongly coupled dimers of DPIBF, a charge separated state has been advocated to act as an intermediate state in the SF process,[51,52] whereas in more weakly coupled dimers charge separation appears to be more of a loss channel.[17,51] More knowledge about the SF process of molecules attached to mesoporous semiconductor surfaces as well as a detailed understanding of the injection dynamics in such molecular−semiconductor assemblies is necessary to gain information about what governs SF and if/how created triplets can be utilized in a device.

Here, we have synthesized two DPIBF derivatives and studied the excited state processes, including SF and electron injection when they are attached to mesoporous nanocrystalline thin films of three different metal oxides. The DPIBF derivatives, Scheme 1, have saturated and flexible carbon linkers with five or six carbons (**C5** and **C6**, respectively) to allow for flexibility in packing on the surfaces and to slow down electron injection from the singlet excited state. The carbon linkers are terminated with a carboxylic acid group to allow for adherence to the metal oxide surfaces. The molecule−semiconductor assemblies are studied in solvents of varying polarity to investigate the role of a potential molecular charge separated state. Three different metal oxide surfaces with different conduction band (CB) energy levels are used: ZrO_2, TiO_2, and SnO_2 (Scheme 1). This allows us to investigate the SF dynamics when the molecules are attached to a mesoporous surface as well as charge injection and recombination dynamics with different driving forces.

Scheme 1. Schematic Energy Diagram Including the Singlet and Triplet Excited State Oxidation Potential of the DPIBF Derivatives in Acetonitrile[a] (C5, n = 4 and C6, n = 5) Together with the CB Energy Levels of the Semiconductors[b]

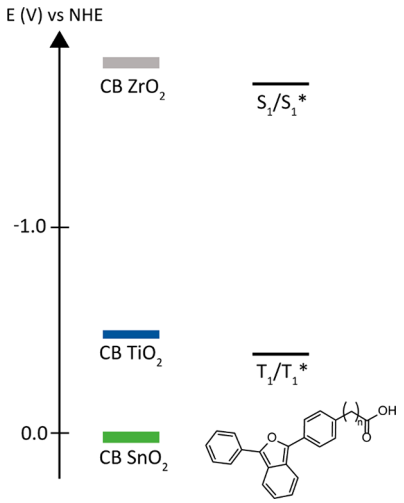

[a]Obtained using the formulas $E^*_{1/2,S1} = E^{ox}_{1/2} - \Delta G_{S1}$ and $E^*_{1/2,T1} = E^{ox}_{1/2} - \Delta G_{T1}$. $E^{ox}_{1/2}$ is assumed to be the same as for unmodified DPIBF;[47] the excited state energy of the S_1 state (ΔG_{S1}) is obtained from the intersection of the normalized absorption and emission spectra, and the excited state energy of the T_1 state (ΔG_{T1}) is assumed to be the same as for unmodified DPIBF.[50] [b]The CB energy level of ZrO_2 is taken from ref 53 and the CB energy levels of TiO_2 and SnO_2 are from ref 54.

EXPERIMENTAL SECTION

Materials. ZrO_2 and SnO_2 pastes were prepared following previously published methods,[55,56] while a commercially available TiO_2 paste (Dyesol 18NR-T) was used. Glass slides (Ted Pella, Inc.) were cleaned by ultrasonication in a 2% RBS 25 detergent (Sigma-Aldrich) solution followed by ultrasonication in acetone prior to use. The solvents (anhydrous) used in the photophysical measurements were purchased from Sigma-Aldrich, degassed, and stored in a nitrogen glovebox prior to use. $Ru(bpy)_2(4,4'\text{-}(COOH)_2bpy)(PF_6)_2$ (Ru455) was purchased from Solaronix, and platinum octaethylporphyr-

https://dx.doi.org/10.1021/acs.jpcc.0c06626
J. Phys. Chem. C 2020, 124, 20794−20805

Scheme 2. Synthesis of C5 and C6

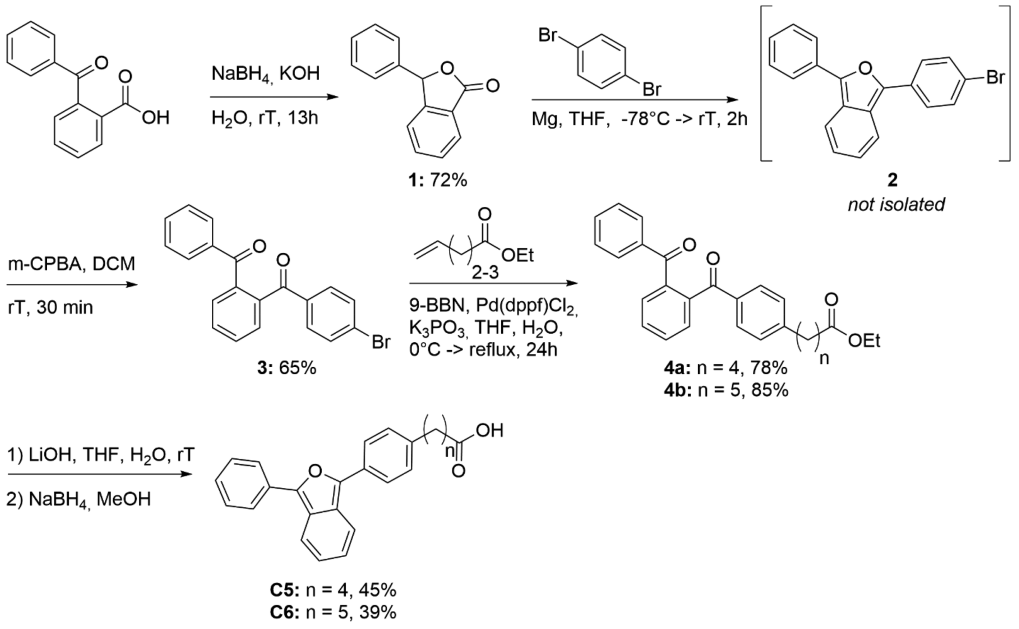

in (PtOEP) was purchased from Sigma-Aldrich and used as received. Starting materials for the synthesis were purchased from commercial vendors and used as received unless otherwise noted.

Synthesis. Methods for organic synthesis as well as proton and carbon NMR spectra of the compounds are described in the Supporting Information, pages S3−S14.

Film Preparation and Characterization. Thin films of the semiconductors were prepared by doctor blading the pastes onto glass substrates with the Scotch tape method, using one layer of tape. The films were then progressively heated to 450 °C and sintered for 30 min. The thickness of the films was measured with a Dektak 150 surface profilometer. The specific surface area of the films was determined by nitrogen adsorption−desorption isotherms at 77 K (Micromeritics Tristar 3000, Norcross GA, USA) using the Brunauer−Emmett−Teller (BET) method at a relative pressure interval of 0.057−0.250. The films were scratched off of the glass and dried under a nitrogen flow, first at 150 °C for 1.5 h followed by 250 °C for 4 h prior to the measurement.

Sample Preparation. All samples were prepared and stored under an inert atmosphere in a glovebox. To sensitize the semiconductor thin films, solutions of various concentrations of the DPIBF derivatives in methanol or toluene were prepared, and the films were placed in these solutions overnight. The films were subsequently rinsed with methanol or toluene, dried in N_2, and placed in sealable 2 mm cuvettes filled with the solvents for the measurement. The surface coverage, Γ (mol/cm^2), of the films was calculated using the formula

$$\Gamma = \frac{A}{\varepsilon_{max} 1000}$$

where ε_{max} is the molar extinction coefficient of the maximum absorption peak of DPIBF in solution (22 900 M^{-1} cm^{-1})[57] and A is the absorbance of the films. The surface coverage was varied by changing the concentration of the solutions. A concentration of 800 μM **C6** in methanol resulted in a fully loaded ZrO_2 film with a surface coverage of ∼100 nmol/cm^2 depending on the film thickness, and a concentration of 45 μM resulted in surface coverages of ∼10 nmol/cm^2. To cosensitize ZrO_2 films with **C6** and Ru455 for the triplet sensitization experiments, the ZrO_2 film was first placed in a methanol solution of Ru455 and subsequently immersed in a toluene solution of **C6**.

Photophysical Measurements. Steady-state absorption spectra were obtained using a Varian-Cary 50 Bio UV−vis spectrophotometer; steady-state emission spectra were obtained with a Spex Fluorolog 3 from JY Horiba. Emission lifetimes were measured with time correlated single photon counting (TCSPC) with a 405 nm pulsed diode laser from PicoQuant as excitation source, and a MCP-PMT detector, using 1024 channels and 5000 counts collected in the top channel. Nanosecond transient absorption was measured with a Spectra-Physics Nd:YAG laser together with a Spectra-Physics Primoscan optical parametric oscillator (OPO) as excitation source (∼0.5−1 mJ/pulse for spectra and 0.5−2 mJ/pulse for single wavelength traces). To record the nanosecond transient spectra, an Edinburgh Instrument LP 980 spectrometer with an image intensified CCD camera (ICCD, Andor DH320T-25F-03) was used. For the single wavelength traces, data was collected with a Costronics photodetector amplified by a Costronics optical transient amplifier connected to a Tektronix TDS 2022 oscilloscope; the probe light was generated with a quartz tungsten halogen lamp (Ushio) powered by a radiometric power supply (Newport), and the probe wavelength was determined with a Cornerstone 130 monochromator (Oriel Instruments). For femtosecond transient absorption measurements, a Ti:sapphire oscillator (Tsunami, Spectra Physics) was used as seed to a Ti:sapphire regenerative amplifier (Spitfire, Spectra Physics) pumped by a frequency-doubled diode-pumped Nd:YLF laser (Evolution-X, Spectra Physics). This produced pulses of around 200 fs duration (fwhm) at a 1 kHz repetition rate; the laser beam (800 nm) from the amplifier was split, and the two beams were used as pump and probe light. An optical parametric amplifier (OPA) (TOPAS, Light Conversion Ltd.) was used to tune the pump wavelength to yield 400 nm (∼0.4−1 μJ/pulse at the

https://dx.doi.org/10.1021/acs.jpcc.0c06626
J. Phys. Chem. C 2020, 124, 20794−20805

sample). The probe light was focused on a rotating CaF_2 plate to generate a white light continuum, and the pump beam was delayed with respect to the probe beam with an optical delay stage (range 0−10 ns). The white light was split into a probe and reference beam, and the probe beam was overlapped with the pump at the sample. The sample was continuously moved during the measurement to prevent damage to the sample using a home-built sample holder. The probe and reference beam were focused on the entrance slit of a spectrograph and detected by a CCD camera (iXon-Andor) operating synchronously with the 1 kHz laser. The transient spectra were obtained from the difference of the probe light divided by the reference with and without excitation of the sample by the pump beam; 2000 spectra were averaged per delay time using a home written LabVIEW program controlling the setup.

RESULTS

Synthesis and Characterization. The carboxylic acid tethered DPIBF derivatives were synthesized in a six-step linear sequence starting from commercially available 2-benzoylbenzoic acid (Scheme 2). The synthesis was initiated by a reductive lactonization, transforming 2-benzoylbenzoic acid to lactone **1** in good yield. Compound **1** was next treated with 4-bromophenylmagnesium bromide, preformed from the corresponding dibromide and metallic magnesium. The formed Grignard intermediate underwent a ring-forming dehydration upon acidic workup, yielding DPIBF derivative **2**. However, the light and oxygen sensitive nature of the DPIBF core prevented **2** from being a suitable intermediate with two synthetic transformations remaining. Instead, m-CPBA was used to purposely oxidize the DPIBF core to diketone **3** before isolation. Diketone **3** can in this instance be considered as a "protected" form of DPIBF that can be reverted back to the cyclized core under reductive conditions. The aliphatic linkers were thereafter successfully installed via Suzuki reactions. With fresh preparation of the organoborane coupling partners through hydroborations of alkeneoates with 9-BBN, the desired products **4a** and **4b** were obtained in high yields. At last, hydrolysis of the esters and re-formation of the DPIBF cores under reductive conditions with an acidic workup produced **C5** and **C6** in moderate yields. Unreacted starting material could also be isolated and recycled. Installing the sensitive DPIBF structure at the very last step ensured that pure, high-quality chromophores were obtained, as evident by NMR spectra, Figures S6−S7.

Comparison between C5 and C6. Initial photophysical measurements of **C5** and **C6**, both in fluid solution and attached to semiconductor surfaces, resulted in almost identical results for all measurements, suggesting that the minor change in the length of the carbon chain does not result in any changes, neither for the interaction between the DPIBF cores nor for the interaction with the semiconductor. Therefore, only the photophysical measurements of **C6** will be presented in the following sections. Absorption and emission spectra as well as time-resolved emission of **C5** are shown together with the corresponding measurements of **C6** in Figure S8.

Photophysical Properties of C6 in Fluid Solution. UV−vis absorption and emission of **C6** are identical to those of unmodified DPIBF in toluene with absorption and emission maxima at ∼420 and ∼460 nm, respectively, and a fluorescence lifetime of 4.6 ns, Figure 1a,b. This is in good agreement with previous reports of DPIBF photophysics.[50] The fluorescence quantum yield is close to unity in a dilute solution of **C6**,

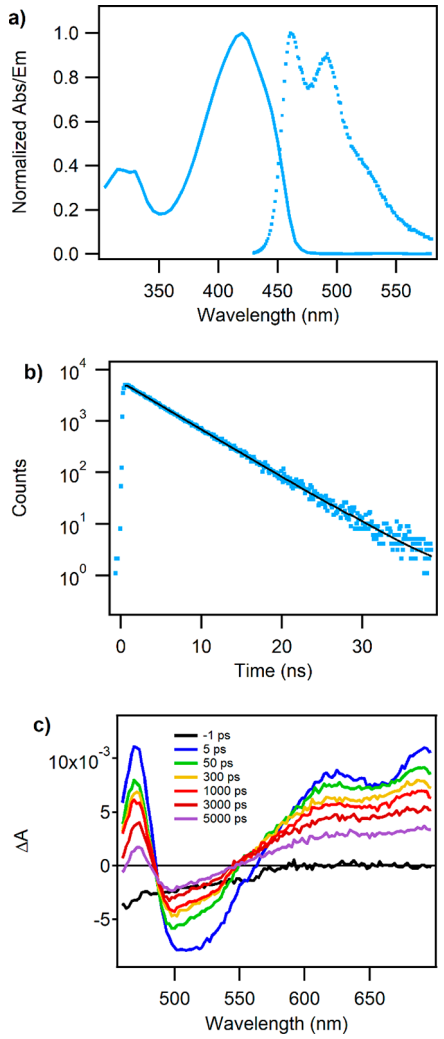

Figure 1. (a) Normalized absorption and steady-state emission spectrum of **C6** in toluene. (b) Time-resolved emission at 500 nm of **C6** in toluene (λ_{exc} = 405 nm) and corresponding monoexponential fit. (c) fs-TA spectra of **C6** (∼70 μM in toluene) (λ_{exc} = 400 nm).

proving that the carbon chain modification does not interfere with any intra- or intermolecular interactions that affect the photophysical properties.

The femtosecond transient absorption (fs-TA) measurement of **C6** in toluene reveals excited state absorption at ∼475 and ∼675 nm that overlaps with the stimulated emission, Figure 1c. The signals at 475 and 675 nm decay uniformly with biexponential kinetics and are attributed to the first singlet excited state in agreement with literature reports.[21] The lifetimes obtained from the trace at 650 nm are 0.14 (9%) and 5.6 (91%) ns (Figure S9) in good agreement with previously reported lifetimes for the singlet excited state[21] as well as the emission lifetime obtained from TCSPC measurements (vide supra). No ISC to long-lived triplets is observed, consistent with the high fluorescence quantum yield.

Spectroscopic Characterization of C6/ZrO_2 Thin Films. When attaching **C6** to thin films of mesoporous nanocrystalline metal oxide semiconductors with a sufficiently high surface coverage, the molecules are expected to be close enough to allow for SF.[1,41] ZrO_2 is often used as a reference material since typically the CB level of ZrO_2 is higher in energy than the S_1 state of many chromophores, and thus, no electron

https://dx.doi.org/10.1021/acs.jpcc.0c06626
J. Phys. Chem. C 2020, 124, 20794−20805

injection into the CB is expected.[58−60] This is true also for **C6** (see Scheme 1), and hence, we can use ZrO_2 to selectively study intermolecular interactions between the **C6** moieties. Thin films of mesoporous nanocrystalline ZrO_2 were prepared as previously described;[56] the surface area of the films was measured to ∼80 m^2/g, and the thickness was ∼3 μm. Sensitization with **C6** was achieved by placing the films in methanol solutions of various concentrations of **C6** overnight. Center-to-center distance between the molecules was estimated to 8 Å for a fully loaded sample (100 $nmol/cm^2$) using previously published methods and assuming hexagonal packing of the molecules.[61]

Figure 2 shows absorption as well as steady-state and time-resolved emission of **C6**/ZrO_2 immersed in toluene. The

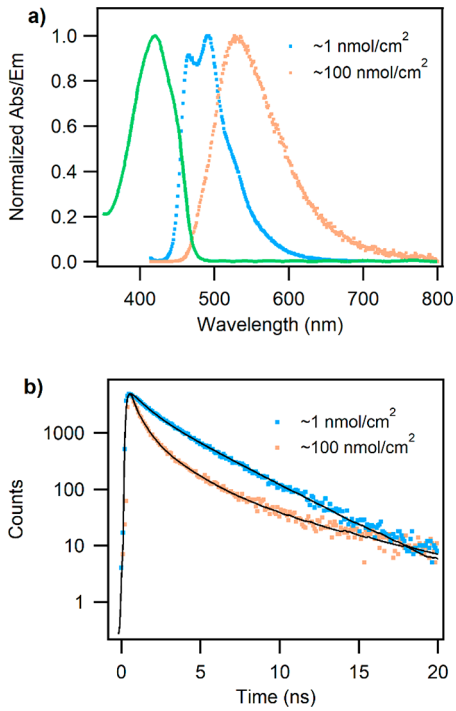

Figure 2. (a) Normalized absorption (green) and emission (orange and blue) spectra of **C6**/ZrO_2 immersed in toluene and (b) effect of surface coverage of **C6**/ZrO_2 immersed in toluene on the emission decay at 500 nm and corresponding fit (λ_{exc} = 405 nm).

absorption spectra of **C6**/ZrO_2 are similar to the solution spectra, but a slight peak-broadening is observed. In contrast, the emission is red-shifted, and the shift increases with increasing surface coverage. Similar observations for DPIBF have previously been attributed to emission from an excimer state[21,41,48] but could also partly be explained by reabsorption of the emission due to the high optical density and broadened absorption of high-surface-coverage samples.

The fluorescence is substantially quenched for **C6**/ZrO_2 immersed in toluene compared to **C6** in fluid solution, and the higher the surface coverage is, the more prominent the quenching is (Table S1), suggesting that intermolecular interactions occur on the surface. The trend is the same also for **C6**/ZrO_2 thin films immersed in neat acetonitrile (MeCN) as well as for solvent free films in a N_2 atmosphere. The number of components required to satisfactorily fit the fluorescence decays also increases with increasing surface coverage. High-surface-coverage samples require at least four components, and a large part of the decay belongs to the two shortest components. A fraction of the decay has a lifetime that is longer-lived than the unquenched lifetime in solution (see Table S1), possibly originating from delayed fluorescence caused by triplet−triplet annihilation following SF. It could also originate from an excimer state, as has been seen upon photoexcitation of DPIBF attached to ZrO_2[41] and recently also in other molecules attached to metal oxide surfaces.[25,62] The emission probed at 700 nm is shown in Figure S10 and confirms the presence of a long-lived species at longer wavelengths.

The highly quenched emission observed for **C6**/ZrO_2 prompted us to perform fs-TA measurements to investigate how the excited state manifold evolves and whether singlet fission occurs on the surface. To conclusively identify the triplet spectral features, triplet sensitization experiments were performed, both on **C6**/ZrO_2 samples where Ru455 was used as the triplet sensitizer, and in solution with PtOEP as the triplet sensitizer (Figures S11 and S12). The triplet state exhibits an excited state absorption peak around ∼460 nm both in toluene solution and when attached to a ZrO_2 surface, similar to what has been previously reported.[50]

fs-TA measurements of **C6**/ZrO_2 were performed in both MeCN (ε = 37.5) and toluene (ε = 2.38) to investigate the effect of solvent polarity, and the fs-TA spectra are presented in Figure 3. At early times, the signals mimic the solution spectra with the expected excited state absorption at 475 and 675 nm, attributed to the absorption of the S_1 state. These features decay much faster than in solution (the decay traces at 675 nm are shown in Figure S13 and require four components for a satisfactory fit in both solvents, Table S2). The majority of the

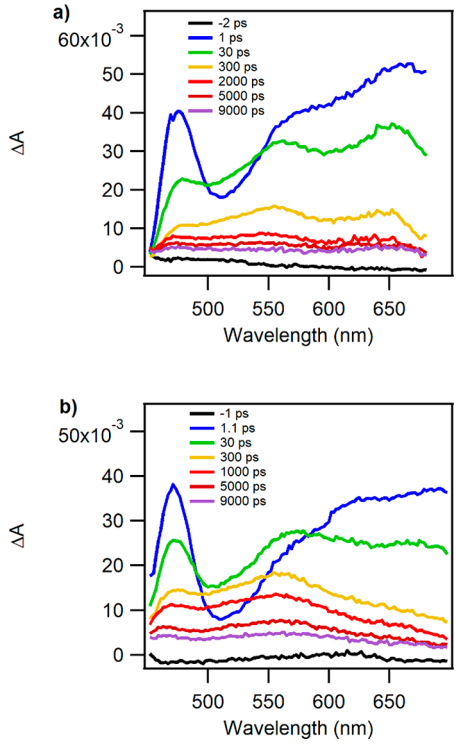

Figure 3. fs-TA spectra of **C6**/ZrO_2 (λ_{exc} = 400 nm) ∼ 90 $nmol/cm^2$ in (a) MeCN and (b) toluene. The region below 450 nm is not included due to the high optical density of the samples that prevents this part of the white light from passing through the samples and into the detector.

https://dx.doi.org/10.1021/acs.jpcc.0c06626
J. Phys. Chem. C 2020, 124, 20794−20805

decay belongs to the shortest component in both solvents, which is faster than 1 ps. At longer times, the spectrum is dominated by signals that are more long-lived than the singlet excited state observed in solution. In MeCN (Figure 3a), new features appear after ~30 ps, centered at 550 and 650 nm which match previous reports of the DPIBF radical cation and anion, respectively,[50] suggesting that a charge separated state between two **C6** molecules is formed, $C6^+/C6^-$. The 550 and 650 nm features appear to mostly decay back to the ground state. After ~2 ns, it is possible to distinguish a shift in the excited state absorption into a weak feature at 460 nm, which probably corresponds to triplets formed via SF. The SF most likely occurs in parallel with the formation of the charge separated state but with a lower efficiency. An alternative explanation for the triplet signal could be that the charge separated state serves as a nonefficient intermediate for the SF process on the surface. In toluene, the spectra look markedly different as can be seen in Figure 3b. There are fewer indications of a $C6^+/C6^-$ state, and importantly, a more distinct excited state feature at 460 nm originating from the triplet excited state is visible after ~1 ns, thus suggesting that SF occurs to a larger extent in toluene.

Since the fs-TA spectra reveal long-lived signals that extend throughout the 10 ns time window, nanosecond transient absorption (ns-TA) of **C6**/ZrO_2 was also performed in the different solvents, Figure 4. The ns-spectra reveal weak triplet

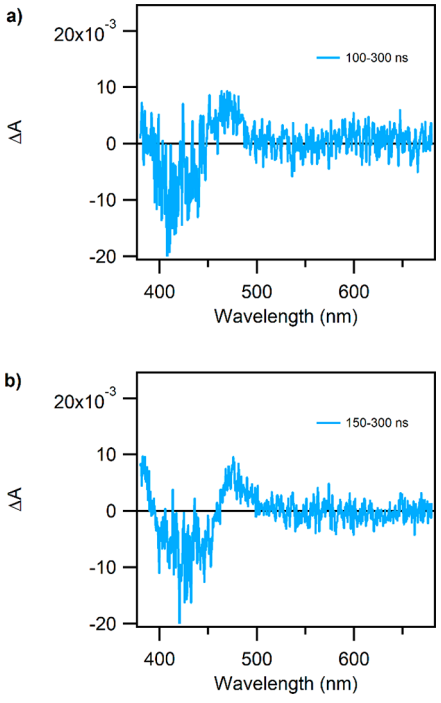

Figure 4. ns-TA spectra of **C6**/ZrO_2 (λ_{exc} = 410 nm) in (a) MeCN (~50 nmol/cm^2) and (b) toluene (~70 nmol/cm^2).

excited state absorption at ~460 nm in both solvents, confirming that triplets are formed, and that they are the most long-lived species. The spectra of the triplet excited state decay uniformly with biexponential kinetics (Figure S14), and the longer component has a lifetime of >200 μs, in good agreement with previously reported lifetimes of the triplet excited state of DPIBF.[50]

Spectroscopic Characterization of C6/TiO_2 Thin Films. When the molecules are attached to mesoporous nanocrystalline TiO_2, singlet injection into the CB of TiO_2 is energetically possible, and as can be seen in Scheme 1, the CB level of TiO_2 and the T_1 level of **C6** are similar in energy. Thus, a competition between electron injection from the singlet excited state and SF can be anticipated, and triplet injection following SF should also be considered. The surface area of the TiO_2 films was measured to be ~70 m^2/g, and the thickness of the films was ~5−6 μm.

The absorption and emission spectra of **C6**/TiO_2 look similar to the **C6**/ZrO_2 spectra (Figure S15a). In contrast, both the steady-state and time-resolved emission are strongly quenched already at low surface coverages (Figure S15b). The high degree of quenching of all samples, together with the lack of concentration dependence, indicates efficient singlet electron injection despite the flexible carbon chain linker.

Femtosecond TA spectra of **C6**/TiO_2 thin films immersed in MeCN and toluene are presented in Figure 5. As can be

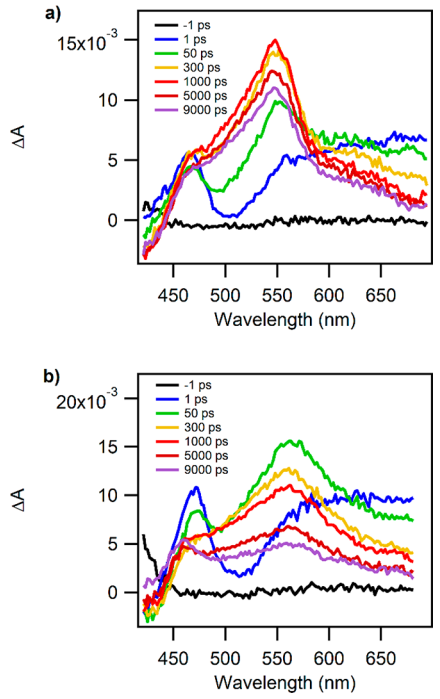

Figure 5. fs-TA spectra of **C6**/TiO_2 (λ_{exc} = 400 nm) ~ 10 nmol/cm^2 in (a) MeCN and (b) toluene.

seen, a charge separated $C6^+/TiO_2(e^-)$ state is rapidly formed in both solvents, resulting from electron injection from the first singlet excited state. This is evident by the rise of a peak at 550 nm, corresponding to the radical cation of **C6**, and a simultaneous fast decay of the singlet excited state, and is consistent with the high degree of quenching observed in the TCSPC measurements. The peak at 550 nm is less intense in toluene compared to in MeCN, suggesting a lower injection yield. Through a comparison of the intensity of the peaks from the singlet excited state and the peak from the radical cation, the injection yield was estimated to be ~15% lower in toluene than in MeCN. No feature at 650 nm is observed; hence, formation of any appreciable concentration of a $C6^+/C6^-$ state can be excluded.

After the initial rise of the peak at 550 nm, the fs-TA spectra have drastically different evolutions in the two solvents. First, the radical cation of **C6** appears to be much longer-lived in MeCN, and the decay during the first 10 ns is almost

https://dx.doi.org/10.1021/acs.jpcc.0c06626
J. Phys. Chem. C 2020, 124, 20794−20805

negligible. In toluene, however, the radical cation starts to decay during the first few nanoseconds after excitation. Moreover, a new feature at 460 nm that matches the triplet excited state appears concomitant with the decay at 550 nm. Since the triplet excited state absorption forms as the signal from the radical cation disappears, a plausible explanation is that the triplet is formed through charge recombination from the CB of TiO_2 to the triplet excited state. It is possible that the lower polarity of toluene destabilizes the **C6**$^+$/TiO_2(e^-) state, making this recombination pathway possible.

To investigate the fate of the excitation at longer time scales, ns-TA spectra were also recorded and are presented in Figure 6. In MeCN, the spectra reveal that the **C6**$^+$/TiO_2(e^-) charge

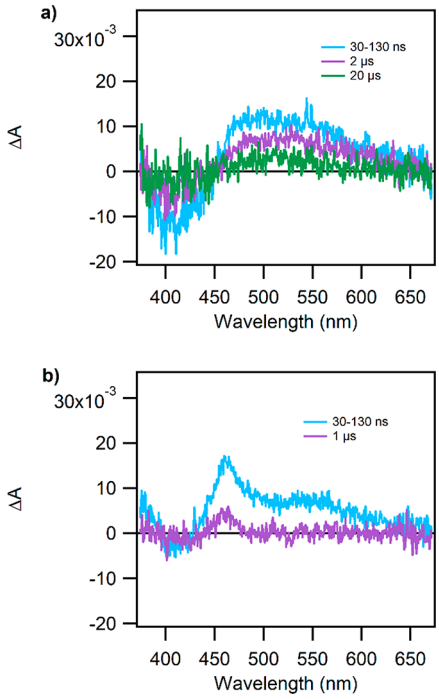

Figure 6. ns-TA spectra of **C6**/TiO_2 (λ_{exc} = 410 nm) in (a) MeCN (~30 nmol/cm^2) and (b) toluene (~10 nmol/cm^2).

separated state is sustained over microsecond time scales since it exhibits the same shape as the final spectra from the fs-TA measurements (Figure 6a). The **C6**$^+$/TiO_2(e^-) peak at 550 nm decays uniformly over the whole spectral range with biexponential kinetics in the microsecond time range (Figure S16a), confirming singlet injection followed by a recombination to the ground state.

In toluene, at ~100 ns after excitation, both the radical cation and the triplet excited state absorption can be distinguished, while at 1 μs the radical cation has decayed completely leaving only the signal from the triplet excited state (Figure 6b). Moreover, the kinetics from the traces at 470 and 550 nm in toluene are different, suggesting that they originate from different species (Figure S16b). This further corroborates that there is charge recombination to the triplet excited state since it is the most long-lived species on the surface.

No indications of SF followed by electron injection from a triplet state are observed for the **C6**/TiO_2 samples in either of the solvents, possibly due to the efficient singlet injection and/or the fact that the triplet excited state is similar in energy as the CB energy level of TiO_2. To ensure that triplet injection is thermodynamically feasible, the same experiment was performed in a 0.1 M $LiClO_4$/MeCN solution, since Li^+ is known to lower the CB energy of TiO_2.[63] This, however, yielded almost identical results as when the sample was immersed in neat MeCN (Figure S17), suggesting that efficient singlet electron injection is the main reason for the lack of SF and triplet injection in **C6**/TiO_2.

Spectroscopic Characterization of C6/SnO_2 Thin Films. When the molecules are attached to mesoporous nanocrystalline SnO_2, both singlet and triplet injection from **C6** into the CB of SnO_2 are energetically feasible, Scheme 1, while charge recombination from the CB to the triplet excited state should be negligible. The surface area of the SnO_2 films was measured to be ~70 m^2/g and the thickness ~3 μm.

The absorption and emission spectra of **C6**/SnO_2 are similar to those of **C6**/ZrO_2 and **C6**/TiO_2 (Figure S18a). As for **C6**/TiO_2, the fluorescence is highly quenched for all investigated surface coverages (Figure S18b). However, the quenching for low-surface-coverage samples is smaller than that for comparable surface coverages on TiO_2. The lower degree of quenching for low-surface-coverage samples indicates a lower injection yield and a possibility that SF contributes to the higher degree of quenching in samples with higher surface coverages.

The fs-TA spectra of **C6**/SnO_2 immersed in MeCN and toluene are presented in Figure 7 and reveal both some

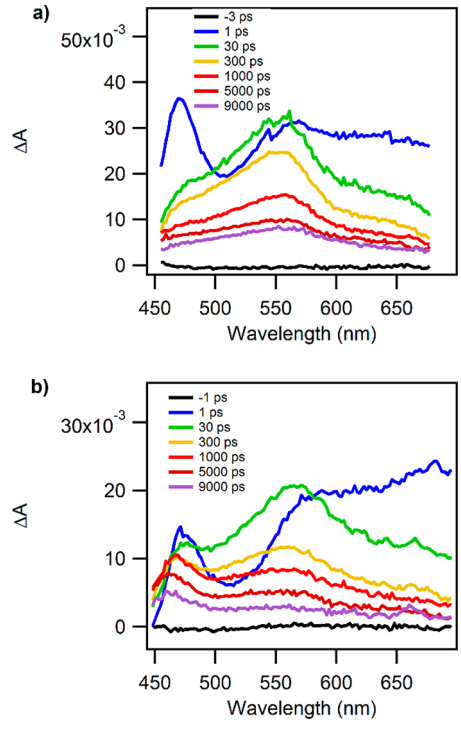

Figure 7. fs-TA spectra of **C6**/SnO_2 (λ_{exc} = 400 nm) in (a) MeCN (~80 nmol/cm^2) and (b) toluene (~40 nmol/cm^2).

similarities and some intriguing differences. In both solvents, the singlet excited state decays rapidly and concomitantly with the rise of the **C6** radical cation signature at 550 nm indicating singlet electron injection that yields **C6**$^+$/SnO_2(e^-). The peak from the radical cation is less intense compared to that for **C6**/TiO_2 in both solvents, pointing to a lower injection yield on SnO_2. The radical cation signature for **C6**/SnO_2 moreover starts to decay during the first few nanoseconds, suggesting a faster recombination to the ground state than was observed on

https://dx.doi.org/10.1021/acs.jpcc.0c06626
J. Phys. Chem. C 2020, 124, 20794−20805

TiO_2. This agrees with previously observed differences in interfacial charge recombination rates of dye-sensitized TiO_2 and SnO_2 electrodes.[64]

Looking instead at the region around 450−500 nm, the spectra evolve differently in the two solvents. In toluene, a feature at 460 nm grows in while in MeCN the radical cation is the only feature that is observed in the femtosecond spectra. The peak at 460 nm corresponds to the triplet excited state absorption of **C6**, and these triplets are likely formed via SF. This suggests that when **C6**/SnO_2 is immersed in toluene, SF partly outcompetes singlet injection and that the two processes occur in parallel.

Nanosecond TA spectra of **C6**/SnO_2 thin films are shown in Figure 8, and interestingly, it is dominated by a broad signal at

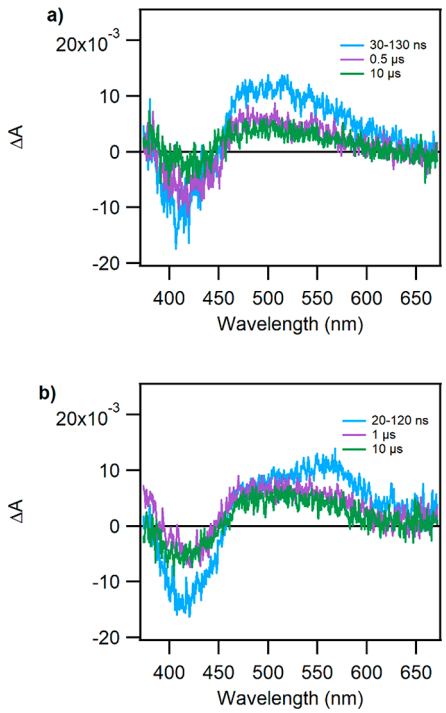

Figure 8. ns-TA spectra of **C6**/SnO_2 (λ_{exc} = 410 nm) in (a) MeCN (~40 nmol/cm^2) and (b) toluene (~20 nmol/cm^2).

450−550 nm in both solvents that mainly matches the signal from the radical cation. This is not surprising in MeCN and likely results from the initially formed **C6**$^+$/SnO_2(e^-) charge separated state that recombines to the ground state. In toluene, however, the triplet excited state that dominated the final spectra in the fs-TA measurements has evolved into the radical cation. This is attributed to triplet electron injection into the CB of SnO_2, demonstrating that triplets formed via SF can inject electrons into the CB. The signal at 550 nm decays to the ground state with the same lifetimes in both solvents which is on the order of microseconds (Figure S19). The slightly broadened absorption in the 450−500 nm region could be the result of a few residual triplets formed via SF that did not inject electrons into the CB. This explanation is confirmed by the decay at 470 nm which is similar to the observed triplet decay on ZrO_2 and markedly different from the decay at 550 nm (Figure S19), thus suggesting that SF occurs in both solvents but to a lower degree in MeCN.

DISCUSSION

Scheme 3 illustrates the events following photoexcitation of **C6** attached to the metal oxide thin films in MeCN and toluene. The scheme includes the energies of the charge separated state between the **C6** molecules, **C6**$^+$/**C6**$^-$, that could either facilitate or hamper the singlet fission process.[16,51,65] The relationships between the oxidation potential of the singlet and triplet excited state and the CB energy level of the different semiconductors are also included in the scheme. The **C6**$^+$/**C6**$^-$ energies in the different solvents were calculated using the Rehm−Weller equation,[66,67] assuming that a **C6** molecule can be approximated with a 4 Å radius and that the distance between molecules is 8 Å, which would be the case for a fully loaded ZrO_2 film with a monolayer of **C6** molecules attached to the surface. The oxidation and reduction potentials are assumed to be the same as for unmodified DPIBF.[47] As can be seen in Scheme 3, the **C6**$^+$/**C6**$^-$ state is lower in energy than the S_1 state in MeCN while it is slightly higher than the S_1 state in toluene. This implies that a molecular charge separated state could be formed upon excitation to the S_1 state in MeCN, while a **C6**$^+$/**C6**$^-$ state is not expected to form in appreciable concentrations upon excitation to the S_1 state in toluene.

The results presented here demonstrates that **C6**/ZrO_2 behaves differently upon photoexcitation depending on whether it is immersed in MeCN or toluene, especially on time scales up to ~10 ns. It is also discernible from the TA spectra and the relatively weak triplet excited state features that the efficiency of the SF process in **C6**/ZrO_2 is rather low and that competing processes, e.g., formation of excimers or charge separation, dominate. Our results suggest that SF does occur to a larger extent in toluene, where the **C6**$^+$/**C6**$^-$ state is not readily accessible, while a more polar environment seems to favor a charge separated state that mainly recombines to the ground state. The solvent dependence is evident by the fs-TA spectra that reveal features corresponding to the radical cation and anion that decays to the ground state in MeCN, while in toluene a more distinct triplet feature can be observed. Hanson and co-workers reported a similar spectral feature for their DPIBF derivative attached to ZrO_2 thin films in MeCN.[41] They assigned the signal to the triplet excited state but noted that the spectra are complex and that a charge separated state is another possibility. To confirm the polarity dependence, measurements in tetrahydrofuran (THF), which has an intermediate polarity that also could result in a **C6**$^+$/**C6**$^-$ state (ε = 7.58 yielding a CSS energy of ~2.8 eV which is similar to the S_1 energy), were performed (Figure S20). Indeed, the fs-TA spectra of **C6**/ZrO_2 in THF reveal formation of a **C6**$^+$/**C6**$^-$ state upon photoexcitation (Figure S20a), with slightly less intense peaks from the radical cation and anion compared to those in MeCN. Moreover, a somewhat more distinct shift in the excited state absorption toward a triplet feature at 460 nm can be distinguished in THF compared to that in MeCN after ~5 ns, although it is still less pronounced than in toluene. As in MeCN, the **C6**$^+$/**C6**$^-$ state in THF mainly returns to the ground state, confirming that a **C6**$^+$/**C6**$^-$ state is favored in polar environments and that it does not act as an efficient intermediate for SF on ZrO_2. However, the formation of a charge separated state does not explain the weak triplet feature that can be distinguished also in more polar environments a few nanoseconds after excitation. Instead, we hypothesize that SF happens in parallel to the formation of the molecular charge separated state, albeit with a much lower

https://dx.doi.org/10.1021/acs.jpcc.0c06626
J. Phys. Chem. C 2020, 124, 20794−20805

Scheme 3. Proposed Pathways upon Photoexcitation of the Different C6/Semiconductor Assemblies in MeCN (Left) and Toluene (Right)[a]

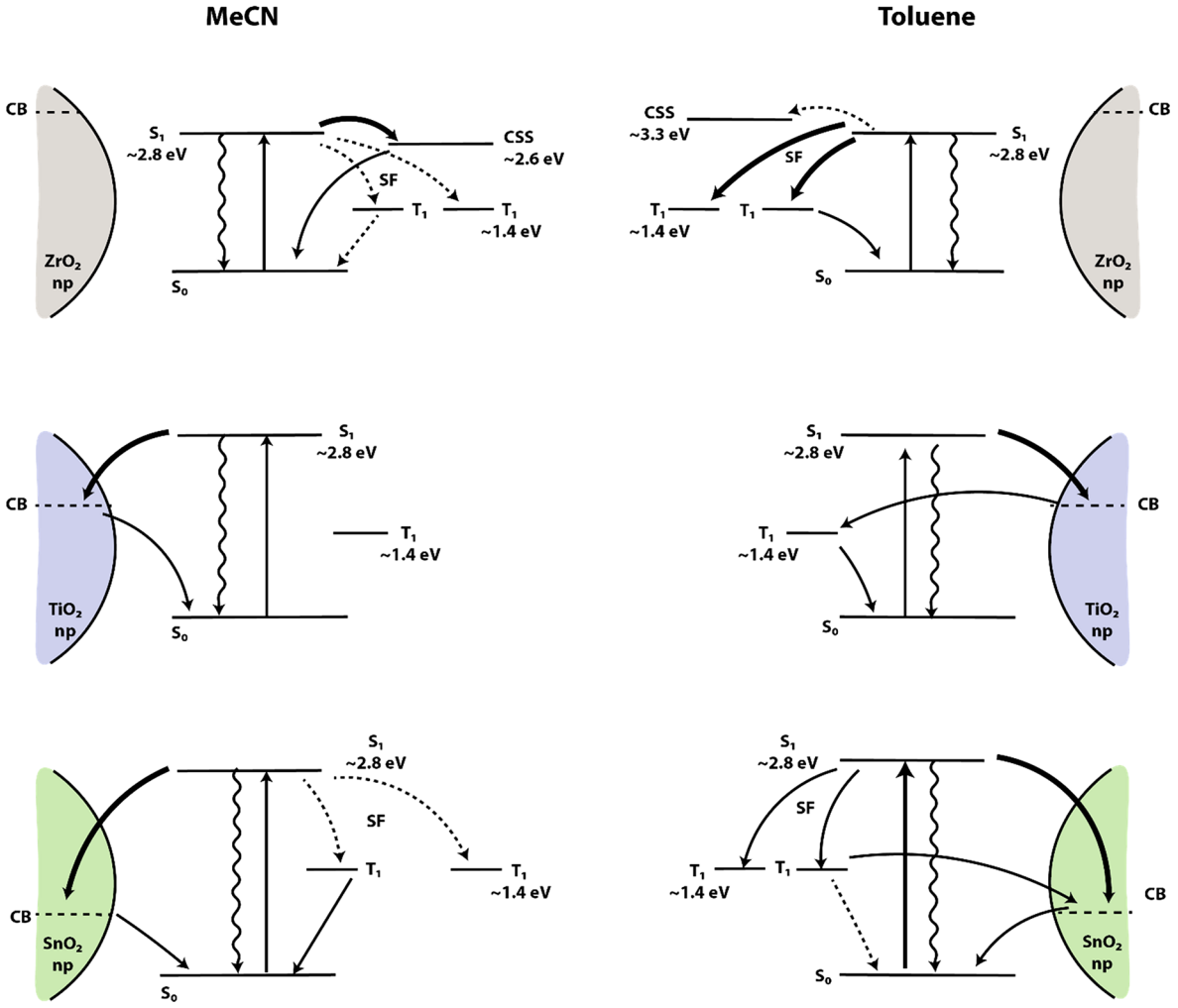

[a]The scheme includes the energy of the S_1 (obtained from the intersection of the normalized absorption and emission spectra) and T_1 (from ref 50 assuming the same T_1 energy as the parent molecule) states of **C6** together with the energy level of the charge separated state (CSS), $\mathbf{C6}^+/\mathbf{C6}^-$, between the **C6** molecules in MeCN and toluene. Solid arrows represent the main pathway, and dotted lines represent a parallel minor pathway. The wavy arrow from S_1 to S_0 represents the remaining weak fluorescence.

efficiency, or that the molecular charge separated state serves as a nonefficient intermediate that leads to SF for only a minority of the molecules. Assuming that the molecules on the surface can be compared with the dimers (vide supra), these results taken together suggest that the DPIBF cores are weakly coupled on the surface.[17,S1,S2]

Given the low efficiency of the SF process in **C6**/ZrO_2 samples, it is not surprising that it is outcompeted by electron injection from S_1 on both TiO_2 and SnO_2 in polar solvents. In toluene, however, triplet formation was observed in addition to singlet electron injection, both on TiO_2 and SnO_2 samples. We hypothesize that the triplet feature observed in **C6**/TiO_2 samples is likely formed via interfacial charge recombination from the $\mathbf{C6}^+/TiO_2(e^-)$ state. Our hypothesis is based on the observation that the injection yield from S_1 is high, resulting in a low probability for SF, and the similar energies of the CB and T_1/T_1^+ (Scheme 1) making electron recombination to the T_1 state plausible. A recombination pathway to the triplet state is further supported by the fact that the triplet signal grows in as the cation decays. In more polar solvents, a delayed triplet formation is not observed, most likely because of a stabilization of the charge separated state between **C6** and TiO_2. An alternative explanation for the triplet formation observed for **C6**/TiO_2 in toluene could be that SF occurs on TiO_2 as well, but that triplet electron injection is slow since it is energetically unfavorable, resulting in triplet states being the most long-lived species on the TiO_2 surface. This explanation can, however, not explain why the radical cation decays much faster in toluene compared to in other environments. Another possibility for the fast decay of the radical cation in toluene could be that the recombination from $\mathbf{C6}^+/TiO_2(e^-)$ to the ground state is faster in toluene compared to in MeCN; however, since the recombination from $\mathbf{C6}^+/SnO_2(e^-)$ to the ground state displays almost identical kinetics in MeCN and toluene, there is no reason to expect this large of a difference for the **C6**/TiO_2 samples. Instead, it is again likely that a weak coupling between the chromophores results in SF being outcompeted by direct singlet electron injection on TiO_2.

In contrast, there is no other reasonable explanation for the triplet formation other than SF when the molecules are

https://dx.doi.org/10.1021/acs.jpcc.0c06626
J. Phys. Chem. C 2020, 124, 20794−20805

attached to SnO_2. That SF occurs to a larger extent for **C6**/SnO_2 in toluene compared to in MeCN is not surprising and could be explained both by a lower degree of stabilization of the **C6**$^+$/SnO_2(e^-) state and because SF on the surface is more efficient in the less polar solvent, as was also observed for **C6**/ZrO_2. Interestingly, these triplets are subsequently injected into the CB of SnO_2 as is evident from the ns-TA data. This observation indicates that triplets formed via SF on the surface indeed can inject electrons into the CB and possibly enhance the efficiency of dye-sensitized solar cells. However, for this to be efficient, the singlet injection needs to be slowed down more than what was achieved with the flexible carbon linker here and speaks in favor of the approach used by, e.g., Johnson[46] and Hanson[41] of using a blocking layer to slow down singlet injection.

Intriguingly, SF appears to be more efficient on SnO_2 compared to on ZrO_2, as the triplet excited state absorption is much more pronounced in the fs-TA spectra of **C6**/SnO_2 than in the spectra of **C6**/ZrO_2, despite the competition with electron injection on SnO_2, while for **C6**/TiO_2, the fast electron injection precludes meaningful comparisons. The reason for this difference between the semiconductors is not clear but could possibly be related to differences in the interaction between the molecules on the different semiconductors. However, since the carbon chain length has no observable effect, it appears that the packing is dominated by the DPIBF cores on all semiconductors, although we cannot exclude small differences originating from differences in particle size and distribution between the different metal oxides. Further structural insight would be needed to conclusively identify the effects originating from the differences of the semiconductors.

CONCLUSIONS

This study of DPIBF derivatives attached to three different metal oxide surfaces with varying CB energy levels has allowed us to investigate both the SF dynamics as well as the electron injection and recombination dynamics at different thermodynamic driving forces. Our results demonstrate that the SF process of the molecules attached to ZrO_2 surfaces is hindered by the formation of a molecular charge separated state in more polar solvents, while a less polar environment makes the SF process more efficient, thus suggesting that the chromophores are weakly coupled even at high surface coverage. A high singlet injection yield on TiO_2 together with the relatively high CB energy level of TiO_2 does not allow for singlet fission followed by triplet injection. However, when the molecules are attached to SnO_2 in a nonpolar environment, SF can partly outcompete singlet injection, thus allowing for triplet injection into the CB of SnO_2. Our results suggest that utilizing semiconductors with a lower CB energy level could make SF competitive and facilitate electron injection from the triplet states and, furthermore, provides direct evidence that triplets formed via singlet fission indeed can inject electrons into the CB given the right conditions. The results presented here demonstrate that molecule−semiconductor assemblies can behave drastically differently depending on the semiconductor and solvent used, and that it is not straightforward to use an inert reference material such as ZrO_2 and expect similar SF behavior when the molecules are attached to other metal oxide surfaces. Furthermore, it is clear that the electronic coupling between the chromophores on the surface must be carefully considered even when using SF materials that are highly efficient in other environments.

ASSOCIATED CONTENT

Supporting Information

The Supporting Information is available free of charge at https://pubs.acs.org/doi/10.1021/acs.jpcc.0c06626.

Description of the organic synthesis, proton and carbon NMR spectra, additional absorption and emission data, additional transient absorption data, and triplet sensitization (PDF)

AUTHOR INFORMATION

Corresponding Author

Maria Abrahamsson − *Department of Chemistry and Chemical Engineering, Chalmers University of Technology, Gothenburg 412 96, Sweden;* orcid.org/0000-0002-6931-1128; Email: abmaria@chalmers.se

Authors

Elin Sundin − *Department of Chemistry and Chemical Engineering, Chalmers University of Technology, Gothenburg 412 96, Sweden*

Rasmus Ringström − *Department of Chemistry and Chemical Engineering, Chalmers University of Technology, Gothenburg 412 96, Sweden*

Fredrik Johansson − *Department of Chemistry and Chemical Engineering, Chalmers University of Technology, Gothenburg 412 96, Sweden*

Betül Küçüköz − *Department of Chemistry and Chemical Engineering, Chalmers University of Technology, Gothenburg 412 96, Sweden*

Andreas Ekebergh − *Department of Chemistry and Chemical Engineering, Chalmers University of Technology, Gothenburg 412 96, Sweden*

Victor Gray − *Department of Chemistry and Chemical Engineering, Chalmers University of Technology, Gothenburg 412 96, Sweden;* orcid.org/0000-0001-6583-8654

Bo Albinsson − *Department of Chemistry and Chemical Engineering, Chalmers University of Technology, Gothenburg 412 96, Sweden;* orcid.org/0000-0002-5991-7863

Jerker Mårtensson − *Department of Chemistry and Chemical Engineering, Chalmers University of Technology, Gothenburg 412 96, Sweden*

Complete contact information is available at: https://pubs.acs.org/10.1021/acs.jpcc.0c06626

Author Contributions

This study was completed through contributions of all authors. All authors have given approval to the final version of the manuscript.

Notes

The authors declare no competing financial interest.

ACKNOWLEDGMENTS

Dr. Joachim Wallenstein is acknowledged for valuable discussions, Felix Hemmingsson for help with BET measurements and Dr. Battulga Munkhbat for help with surface profilometer measurements. Assoc. Prof. Karl Börjesson is acknowledged for providing access to their ns-TA system, and Dr. Chen Ye is acknowledged for assisting during these

measurements. The Swedish Energy Agency provided financial support (grant 36436-2).

REFERENCES

(1) Smith, M. B.; Michl, J. Singlet fission. *Chem. Rev.* **2010**, *110*, 6891−6936.
(2) Geacintov, N.; Pope, M.; Vogel, F. Effect of magnetic field on the fluorescence of tetracene crystals: exciton fission. *Phys. Rev. Lett.* **1969**, *22*, 593−596.
(3) Merrifield, R. E.; Avakian, P.; Groff, R. P. Fission of singlet excitons into pairs of triplet excitons in tetracene crystals. *Chem. Phys. Lett.* **1969**, *3*, 386−388.
(4) Singh, S.; Jones, W. J.; Siebrand, W.; Stoicheff, B. P.; Schneider, W. G. Laser generation of excitons and fluorescence in anthracene crystals. *J. Chem. Phys.* **1965**, *42*, 330−342.
(5) Swenberg, C. E.; Stacy, W. T. Bimolecular radiationless transitions in crystalline tetracene. *Chem. Phys. Lett.* **1968**, *2*, 327−328.
(6) Smith, M. B.; Michl, J. Recent advances in singlet fission. *Annu. Rev. Phys. Chem.* **2013**, *64*, 361−386.
(7) Hanna, M. C.; Nozik, A. J. Solar conversion efficiency of photovoltaic and photoelectrolysis cells with carrier multiplication absorbers. *J. Appl. Phys.* **2006**, *100*, 074510.
(8) Shockley, W.; Queisser, H. J. Detailed balance limit of efficiency of p−n junction solar cells. *J. Appl. Phys.* **1961**, *32*, 510−519.
(9) Lee, J.; Jadhav, P.; Reusswig, P. D.; Yost, S. R.; Thompson, N. J.; Congreve, D. N.; Hontz, E.; Van Voorhis, T.; Baldo, M. A. Singlet exciton fission photovoltaics. *Acc. Chem. Res.* **2013**, *46*, 1300−1311.
(10) Ito, S.; Nagami, T.; Nakano, M. Molecular design for efficient singlet fission. *J. Photochem. Photobiol., C* **2018**, *34*, 85−120.
(11) Piland, G. B.; Burdett, J. J.; Dillon, R. J.; Bardeen, C. J. Singlet fission: From coherences to kinetics. *J. Phys. Chem. Lett.* **2014**, *5*, 2312−2319.
(12) Bakulin, A. A.; Morgan, S. E.; Kehoe, T. B.; Wilson, M. W. B.; Chin, A. W.; Zigmantas, D.; Egorova, D.; Rao, A. Real-time observation of multiexcitonic states in ultrafast singlet fission using coherent 2D electronic spectroscopy. *Nat. Chem.* **2016**, *8*, 16−23.
(13) Pun, A. B.; Asadpoordarvish, A.; Kumarasamy, E.; Tayebjee, M. J. Y; Niesner, D.; McCamey, D. R.; Sanders, S. N.; Campos, L. M.; Sfeir, M. Y. Ultra-fast intramolecular singlet fission to persistent multiexcitons by molecular design. *Nat. Chem.* **2019**, *11*, 821−828.
(14) Low, J. Z.; Sanders, S. N.; Campos, L. M. Correlating structure and function in organic electronics: from single molecule transport to singlet fission. *Chem. Mater.* **2015**, *27*, 5453−5463.
(15) El Bakouri, O.; Smith, J. R.; Ottosson, H. Strategies for design of potential singlet fission chromophores utilizing a combination of ground-state and excited-state aromaticity rules. *J. Am. Chem. Soc.* **2020**, *142*, 5602−5617.
(16) Monahan, N.; Zhu, X.-Y. Charge transfer−mediated singlet fission. *Annu. Rev. Phys. Chem.* **2015**, *66*, 601−618.
(17) Johnson, J. C.; Michl, J. 1, 3-Diphenylisobenzofuran: a model chromophore for singlet fission. *Top. Curr. Chem.* **2017**, *375*, 80.
(18) Margulies, E. A.; Logsdon, J. L.; Miller, C. E.; Ma, L.; Simonoff, E.; Young, R. M.; Schatz, G. C.; Wasielewski, M. R. Direct observation of a charge-transfer state preceding high-yield singlet fission in terrylenediimide thin films. *J. Am. Chem. Soc.* **2017**, *139*, 663−671.
(19) Margulies, E. A.; Miller, C. E.; Wu, Y.; Ma, L.; Schatz, G. C.; Young, R. M.; Wasielewski, M. R. Enabling singlet fission by controlling intramolecular charge transfer in π-stacked covalent terrylenediimide dimers. *Nat. Chem.* **2016**, *8*, 1120−1125.
(20) Dover, C. B.; Gallaher, J. K.; Frazer, L.; Tapping, P. C.; Petty, A. J.; Crossley, M. J.; Anthony, J. E.; Kee, T. W.; Schmidt, T. W. Endothermic singlet fission is hindered by excimer formation. *Nat. Chem.* **2018**, *10*, 305−310.
(21) Dron, P. I.; Michl, J.; Johnson, J. C. Singlet fission and excimer formation in disordered solids of alkyl-substituted 1, 3-diphenylisobenzofurans. *J. Phys. Chem. A* **2017**, *121*, 8596−8603.
(22) Krishnapriya, K. C.; Musser, A. J.; Patil, S. Molecular design strategies for efficient intramolecular singlet exciton fission. *ACS Energy Lett.* **2019**, *4*, 192−202.
(23) Mauck, C. M.; Hartnett, P. E.; Margulies, E. A.; Ma, L.; Miller, C. E.; Schatz, G. C.; Marks, T. J.; Wasielewski, M. R. Singlet fission via an excimer-like intermediate in 3, 6-bis (thiophen-2-yl) diketopyrrolopyrrole derivatives. *J. Am. Chem. Soc.* **2016**, *138*, 11749−11761.
(24) Walker, B. J.; Musser, A. J.; Beljonne, D.; Friend, R. H. Singlet exciton fission in solution. *Nat. Chem.* **2013**, *5*, 1019−1024.
(25) Yu, Y.; Chien, S.-C.; Sun, J.; Hettiaratchy, E. C.; Myers, R. C.; Lin, L.-C.; Wu, Y. Excimer-mediated intermolecular charge transfer in self-assembled donor−acceptor dyes on metal oxides. *J. Am. Chem. Soc.* **2019**, *141*, 8727−8731.
(26) Zimmerman, P. M.; Musgrave, C. B.; Head-Gordon, M. A correlated electron view of singlet fission. *Acc. Chem. Res.* **2013**, *46*, 1339−1347.
(27) Johnson, J. C.; Nozik, A. J.; Michl, J. The role of chromophore coupling in singlet fission. *Acc. Chem. Res.* **2013**, *46*, 1290−1299.
(28) Greyson, E. C.; Vura-Weis, J.; Michl, J.; Ratner, M. A. Maximizing singlet fission in organic dimers: theoretical investigation of triplet yield in the regime of localized excitation and fast coherent electron transfer. *J. Phys. Chem. B* **2010**, *114*, 14168−14177.
(29) Basel, B. S.; Zirzlmeier, J.; Hetzer, C.; Reddy, S. R.; Phelan, B. T.; Krzyaniak, M. D.; Volland, M. K.; Coto, P. B.; Young, R. M.; Clark, T.; et al. Evidence for charge-transfer mediation in the primary events of singlet fission in a weakly coupled pentacene dimer. *Chem.* **2018**, *4*, 1092−1111.
(30) Burdett, J. J.; Müller, A. M.; Gosztola, D.; Bardeen, C. J. Excited state dynamics in solid and monomeric tetracene: The roles of superradiance and exciton fission. *J. Chem. Phys.* **2010**, *133*, 144506.
(31) Eaton, S. W.; Miller, S. A.; Margulies, E. A.; Shoer, L. E.; Schaller, R. D.; Wasielewski, M. R. Singlet exciton fission in thin films of tert-butyl-substituted terrylenes. *J. Phys. Chem. A* **2015**, *119*, 4151−4161.
(32) Johnson, J. C.; Nozik, A. J.; Michl, J. High triplet yield from singlet fission in a thin film of 1, 3-diphenylisobenzofuran. *J. Am. Chem. Soc.* **2010**, *132*, 16302−16303.
(33) Sanders, S. N.; Kumarasamy, E.; Pun, A. B.; Trinh, M. T.; Choi, B.; Xia, J.; Taffet, E. J.; Low, J. Z.; Miller, J. R.; Roy, X.; et al. Quantitative intramolecular singlet fission in bipentacenes. *J. Am. Chem. Soc.* **2015**, *137*, 8965−8972.
(34) Pace, N. A.; Korovina, N. V.; Clikeman, T. T.; Holliday, S.; Granger, D. B.; Carroll, G. M.; Nanayakkara, S. U.; Anthony, J. E.; McCulloch, I.; Strauss, S. H.; et al. Slow charge transfer from pentacene triplet states at the Marcus optimum. *Nat. Chem.* **2020**, *12*, 63−70.
(35) Rao, A.; Friend, R. H. Harnessing singlet exciton fission to break the Shockley−Queisser limit. *Nat. Rev. Mater.* **2017**, *2*, 17063.
(36) Zukun, W.; Wu, R.; Chen, Z.; Ye, L.; Li, H.; Zhu, H. Ultrafast electron transfer before singlet fission and slow triplet state electron transfer in pentacene single crystal/C60 heterostructure. *J. Phys. Chem. A* **2020**, *124*, 4185−4192.
(37) Congreve, D. N.; Lee, J.; Thompson, N. J.; Hontz, E.; Yost, S. R.; Reusswig, P. D.; Bahlke, M. E.; Reineke, S.; Van Voorhis, T.; Baldo, M. A. External quantum efficiency above 100% in a singlet-exciton-fission−based organic photovoltaic cell. *Science* **2013**, *340*, 334−337.
(38) Pazos-Outón, L. M.; Lee, J. M.; Futscher, M. H.; Kirch, A.; Tabachnyk, M.; Friend, R. H.; Ehrler, B. A silicon−singlet fission tandem solar cell exceeding 100% external quantum efficiency with high spectral stability. *ACS Energy Lett.* **2017**, *2*, 476−480.
(39) Thompson, N. J.; Congreve, D. N.; Goldberg, D.; Menon, V. M.; Baldo, M. A. Slow light enhanced singlet exciton fission solar cells with a 126% yield of electrons per photon. *Appl. Phys. Lett.* **2013**, *103*, 263302.
(40) Paci, I.; Johnson, J. C.; Chen, X.; Rana, G.; Popović, D.; David, D. E.; Nozik, A. J.; Ratner, M. A.; Michl, J. Singlet fission for dye-sensitized solar cells: Can a suitable sensitizer be found? *J. Am. Chem. Soc.* **2006**, *128*, 16546−16553.

https://dx.doi.org/10.1021/acs.jpcc.0c06626
J. Phys. Chem. C 2020, 124, 20794−20805

(41) Banerjee, T.; Hill, S. P.; Hermosilla-Palacios, M. A.; Piercy, B. D.; Haney, J.; Casale, B.; DePrince, A. E.; Losego, M. D.; Kleiman, V. D.; Hanson, K. Diphenylisobenzofuran bound to nanocrystalline metal oxides: excimer formation, singlet fission, electron injection, and low energy sensitization. *J. Phys. Chem. C* **2018**, *122*, 28478−28490.
(42) Wang, J. C.; Hill, S. P.; Dilbeck, T.; Ogunsolu, O. O.; Banerjee, T.; Hanson, K. Multimolecular assemblies on high surface area metal oxides and their role in interfacial energy and electron transfer. *Chem. Soc. Rev.* **2018**, *47*, 104−148.
(43) Einzinger, M.; Wu, T.; Kompalla, J. F.; Smith, H. L.; Perkinson, C. F.; Nienhaus, L.; Wieghold, S.; Congreve, D. N.; Kahn, A.; Bawendi, M. G.; et al. Sensitization of silicon by singlet exciton fission in tetracene. *Nature* **2019**, *571*, 90−94.
(44) Kunzmann, A.; Gruber, M.; Casillas, R.; Zirzlmeier, J.; Stanzel, M.; Peukert, W.; Tykwinski, R. R.; Guldi, D. M. Singlet fission for photovoltaics with 130% injection efficiency. *Angew. Chem., Int. Ed.* **2018**, *57*, 10742−10747.
(45) Pace, N. A.; Arias, D. H.; Granger, D. B.; Christensen, S.; Anthony, J. E.; Johnson, J. C. Dynamics of singlet fission and electron injection in self-assembled acene monolayers on titanium dioxide. *Chem. Sci.* **2018**, *9*, 3004−3013.
(46) Schrauben, J. N.; Zhao, Y.; Mercado, C.; Dron, P. I.; Ryerson, J. L.; Michl, J.; Zhu, K.; Johnson, J. C. Photocurrent enhanced by singlet fission in a dye-sensitized solar cell. *ACS Appl. Mater. Interfaces* **2015**, *7*, 2286−2293.
(47) Akdag, A.; Wahab, A.; Beran, P.; Rulisek, L.; Dron, P. I.; Ludvik, J.; Michl, J. Covalent dimers of 1, 3-Diphenylisobenzofuran for singlet fission: synthesis and electrochemistry. *J. Org. Chem.* **2015**, *80*, 80−89.
(48) Ryerson, J. L.; Schrauben, J. N.; Ferguson, A. J.; Sahoo, S. C.; Naumov, P.; Havlas, Z.; Michl, J.; Nozik, A. J.; Johnson, J. C. Two thin film polymorphs of the singlet fission compound 1, 3-diphenylisobenzofuran. *J. Phys. Chem. C* **2014**, *118*, 12121−12132.
(49) Schrauben, J. N.; Ryerson, J. L.; Michl, J.; Johnson, J. C. Mechanism of singlet fission in thin films of 1, 3-diphenylisobenzofuran. *J. Am. Chem. Soc.* **2014**, *136*, 7363−7373.
(50) Schwerin, A. F.; Johnson, J. C.; Smith, M. B.; Sreearunothai, P.; Popovic, D.; Černý, J.; Havlas, Z.; Paci, I.; Akdag, A.; MacLeod, M. K.; et al. Toward designed singlet fission: electronic states and photophysics of 1, 3-diphenylisobenzofuran. *J. Phys. Chem. A* **2010**, *114*, 1457−1473.
(51) Johnson, J. C.; Akdag, A.; Zamadar, M.; Chen, X.; Schwerin, A. F.; Paci, I.; Smith, M. B.; Havlas, Z.; Miller, J. R.; Ratner, M. A.; et al. Toward designed singlet fission: solution photophysics of two indirectly coupled covalent dimers of 1, 3-diphenylisobenzofuran. *J. Phys. Chem. B* **2013**, *117*, 4680−4695.
(52) Schrauben, J. N.; Akdag, A.; Wen, J.; Havlas, Z.; Ryerson, J. L.; Smith, M. B.; Michl, J.; Johnson, J. C. Excitation localization/delocalization isomerism in a strongly coupled covalent dimer of 1, 3-diphenylisobenzofuran. *J. Phys. Chem. A* **2016**, *120*, 3473−3483.
(53) Butler, M. A.; Ginley, D. S. Prediction of flatband potentials at semiconductor-electrolyte interfaces from atomic electronegativities. *J. Electrochem. Soc.* **1978**, *125*, 228−232.
(54) Tiwana, P.; Docampo, P.; Johnston, M. B.; Snaith, H. J.; Herz, L. M. Electron mobility and injection dynamics in mesoporous ZnO, SnO_2, and TiO_2 films used in dye-sensitized solar cells. *ACS Nano* **2011**, *5*, 5158−5166.
(55) Chappel, S.; Zaban, A. Nanoporous SnO_2 electrodes for dye-sensitized solar cells: improved cell performance by the synthesis of 18 nm SnO_2 colloids. *Sol. Energy Mater. Sol. Cells* **2002**, *71*, 141−152.
(56) Heimer, T. A.; D'Arcangelis, S. T.; Farzad, F.; Stipkala, J. M.; Meyer, G. J. An acetylacetonate-based semiconductor- sensitizer linkage. *Inorg. Chem.* **1996**, *35*, 5319−5324.
(57) Zhang, X.-F.; Li, X. The photostability and fluorescence properties of diphenylisobenzofuran. *J. Lumin.* **2011**, *131*, 2263−2266.
(58) Dilbeck, T.; Hill, S. P.; Hanson, K. Harnessing molecular photon upconversion at sub-solar irradiance using dual sensitized self-assembled trilayers. *J. Mater. Chem. A* **2017**, *5*, 11652−11660.
(59) Durrant, J. R.; Haque, S. A.; Palomares, E. Towards optimisation of electron transfer processes in dye sensitised solar cells. *Coord. Chem. Rev.* **2004**, *248*, 1247−1257.
(60) Tachibana, Y.; Moser, J. E.; Grätzel, M.; Klug, D. R.; Durrant, J. R. Subpicosecond interfacial charge separation in dye-sensitized nanocrystalline titanium dioxide films. *J. Phys. Chem.* **1996**, *100*, 20056−20062.
(61) Zhou, Y.; Ayad, S.; Ruchlin, C.; Posey, V.; Hill, S. P.; Wu, Q.; Hanson, K. Examining the role of acceptor molecule structure in self-assembled bilayers: surface loading, stability, energy transfer, and upconverted emission. *Phys. Chem. Chem. Phys.* **2018**, *20*, 20513−20524.
(62) Gorman, J.; Pandya, R.; Allardice, J. R.; Price, M. B.; Schmidt, T. W.; Friend, R. H.; Rao, A.; Davis, N. J. L. K. Excimer formation in carboxylic acid-functionalized perylene diimides attached to silicon dioxide nanoparticles. *J. Phys. Chem. C* **2019**, *123*, 3433−3440.
(63) Watson, D. F.; Meyer, G. J. Cation effects in nanocrystalline solar cells. *Coord. Chem. Rev.* **2004**, *248*, 1391−1406.
(64) Green, A. N. M.; Palomares, E.; Haque, S. A.; Kroon, J. M.; Durrant, J. R. Charge transport versus recombination in dye-sensitized solar cells employing nanocrystalline TiO_2 and SnO_2 films. *J. Phys. Chem. B* **2005**, *109*, 12525−12533.
(65) Ramanan, C.; Smeigh, A. L.; Anthony, J. E.; Marks, T. J.; Wasielewski, M. R. Competition between singlet fission and charge separation in solution-processed blend films of 6, 13-bis (triisopropylsilylethynyl) pentacene with sterically-encumbered perylene-3, 4:9, 10-bis (dicarboximide)s. *J. Am. Chem. Soc.* **2012**, *134*, 386−397.
(66) Rehm, D.; Weller, A. Kinetics of fluorescence quenching by electron and H-atom transfer. *Isr. J. Chem.* **1970**, *8*, 259−271.
(67) Küçüköz, B.; Adinarayana, B.; Osuka, A.; Albinsson, B. Electron transfer reactions in sub-porphyrin−naphthyldiimide dyads. *Phys. Chem. Chem. Phys.* **2019**, *21*, 16477−16485.

https://dx.doi.org/10.1021/acs.jpcc.0c06626
J. Phys. Chem. C 2020, 124, 20794−20805